Ab initio molecular dynamics simulations of oxide-ion disorder in the δ-Bi_2O_3

Chris E. Mohn,[1,2,*] Svein Stølen,[1] Stefan T. Norberg,[3,4] and Stephen Hull[4]
[1]*Department of Chemistry and Centre for Materials Science and Nanotechnology, University of Oslo, P.O. Box 1033 Blindern, N-0315 Oslo, Norway*
[2]*Laboratoire des Colloïdes, Verres et Nanomatériaux, UMR 5587, Université Montpellier II–CNRS, 34095 Montpellier, France*
[3]*Department of Chemical and Biological Engineering, Chalmers University of Technology, SE-412 96 Gothenburg, Sweden*
[4]*The ISIS Facility, STFC Rutherford Appleton Laboratory, Didcot, Oxfordshire OX11 0QX, United Kingdom*
(Received 27 April 2009; revised manuscript received 14 June 2009; published 17 July 2009)

We study in detail the structural, dynamical, and electronic properties of the β and δ phases of Bi_2O_3 using Born-Oppenheimer molecular dynamics together with extensive lattice static simulations at the level of gradient-corrected density-functional theory. The short Bi-O bonds of ~2.1–2.2 Å and the broad peak in the O-Bi-O angular distribution function at ~70° of δ-Bi_2O_3 are in good agreement with those from neutron diffraction, locally resembling the distorted structures of many fully ordered oxides of bismuth under ambient conditions. This places some doubt on structural models where the oxygen vacancies are either distributed at random over a set of "ideal" anion lattice sites or preferentially aligned in pairs at these positions. The irregular local structure of δ-Bi_2O_3 is intimately connected to the pronounced electron density around bismuth, providing evidence for the presence of a sterochemically active "lone pair." The dominant influence of the anion $2p$ orbital on this asymmetry mirrors recent findings for many ordered post-transition-metal oxides and contrasts that of the conventional "ns^2 lone-pair model." The markedly curved diffusion trajectories and an unusually high occurrence of short residence times show that the oxygen diffusion is strongly influenced by the local distortions of the immobile lattice. In contrast, we find little evidence for collective diffusion of oxygens.

DOI: 10.1103/PhysRevB.80.024205 PACS number(s): 71.15.Pd, 66.30.−h

I. INTRODUCTION

The ionic conductivity of the superionic phase of bismuth sesquioxide, δ-Bi_2O_3, which is similar to that of the extreme case of the prototypal anion superionic conductor β-PbF_2 (Ref. 1–5) and almost 2 orders of magnitude higher than the commonly used yttria stabilized zirconia at comparable temperatures, is the highest known among oxides.[6–8] The δ phase of Bi_2O_3 therefore remains a reference material within the field of solid electrolytes[9–12] and provides the benchmark for attempts to design and synthesize new highly conducting oxides to meet the technological application within, for example, solid oxide fuel cells. While the ordered low-temperature phases of Bi_2O_3 [i.e., the α, β,[6,13] γ,[6,14] and ϵ (Ref. 15) phases] possess markedly distorted structures, a feature quite typical for many post-transition-metal oxides, the δ phase itself adopts a highly symmetrical anion-deficient fluorite structure (space group $Fm\bar{3}m$) with oxygens occupying 6/8 of the tetrahedral cavities, leaving 2/8 vacant for diffusion to take place. Early work carried out by Gattow and Schröder[16] suggests that the oxygens are distributed at random over the tetrahedral 8(c) positions (see Fig. 1) of $Fm\bar{3}m$. However, results from neutron-diffraction (ND) experiments[13,17–19] indicate that the oxygens *also* occupy a 32(f) site displaced about 1 Å away from the 8(c) site into (x,x,x) etc. with $x \sim 0.33$ (see Fig. 1). This shift is consistent with ionic distribution profiles extracted from x-ray diffraction[19] which shows that the oxygens are spread out within large regions of the tetrahedral cavities possessing marked distortions in the ⟨111⟩ direction.

Computational and experimental studies have revealed the likelihood of pronounced short-range order within the highly disordered oxygen sublattice,[18,20–25] but there is no clear understanding of how the oxygens/oxygen vacancies prefer to arrange themselves or the lengthscale of this local order. Lattice statics models,[23] diffraction studies,[14,18] and an early density functional theory (DFT) study (carried out using linear muffin-tin orbitals)[24] suggest that the oxygen vacancies prefer to align along the ⟨111⟩ directions (see Fig. 2). On the other hand, recent DFT calculations using the generalized gradient approximation (GGA) (Refs. 20, 26, and 27) show that the ⟨100⟩ oxygen-vacancy alignment has the lowest

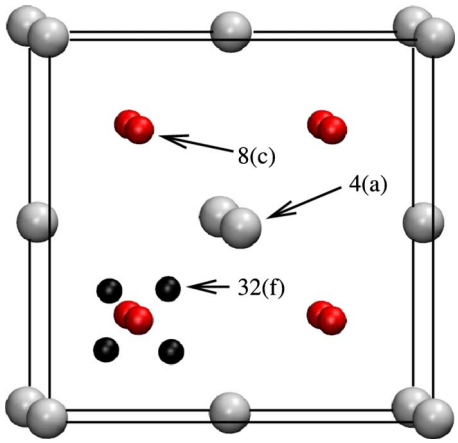

FIG. 1. (Color online) Average positions of bismuths and oxygens within δ-Bi_2O_3 (the refined positions are taken from Ref. 13). The bismuths are shown as large white spheres [at the crystallographic 4(a) site]. The small red and black spheres represent oxygens at the tetrahedral 8(c) and the "interstitial" 32(f) sites which are the site on a straight line connecting the tetrahedral 8(c) and the nearest octahedral 4(b) positions [i.e., at the positions (x,x,x), etc., with x=0.33 (Ref. 13)].

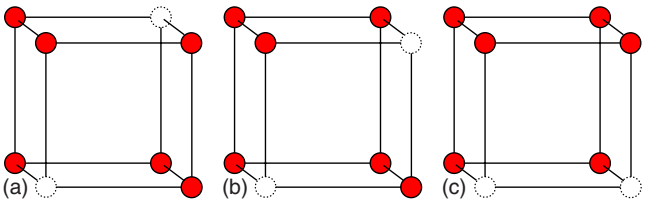

FIG. 2. (Color online) Models of the three distinct vacancy arrangements (marked as dashed white spheres) where the two vacancies are aligned in the ⟨111⟩, ⟨110⟩, and ⟨100⟩ directions. The red spheres are the oxygens.

energy whereas the energy of the ⟨110⟩ configuration is found to be marginally higher. In contrast, recent full-potential linearized augmented plane-wave calculations using GGA (Ref. 22) indicate an energetic preference for the ⟨110⟩ configuration over that of ⟨100⟩. In all these calculations,[20,22,26,27] the ordered ⟨111⟩ configuration was found to be much higher in energy, although lattice static considerations[25] indicate that the introduction of the ⟨110⟩ "defects" within the ⟨111⟩ array could lower the energy of the ordered ⟨111⟩ structure due to substantial local structural relaxations. Indeed, the superstructure suggested in a recent DFT study[21] by embedding ⟨110⟩ and ⟨111⟩ within a 80-ion supercell was found to have significantly lower energy compared to the simple ⟨100⟩ and ⟨110⟩ configurations. However, an ordered superstructure[21] cannot, for example, explain the abrupt increase in the configurational entropy of the phase transition from the fully ordered α phase to the highly disordered δ phase,[28] $\Delta S(\alpha \rightarrow \delta)/[\Delta S(\alpha \rightarrow \delta)+\Delta S(\delta \rightarrow L)]=0.75$, which is more likely to involve a thermal average of a range of different local environments.

Identifying the positions of the oxygens within δ-Bi_2O_3 has important implications for diffusion within this phase. Simple defect considerations for phase stabilized δ-Bi_2O_3 suggest that the oxygen jumps may involve nearest-neighbor tetrahedral cavities possibly via an interstitial 32(f) position.[29] The activation energy for oxide-ion diffusion calculated from DFT (Ref. 26) by mapping the energy for a single oxygen along the ⟨100⟩ direction (i.e., by connecting the local ⟨100⟩ and ⟨110⟩ alignments) was in good agreement with that of conductivity measurements (~0.4 eV).[30] However the activation energy is substantially higher than the heat of transport, $Q=0.13$ eV, estimated from thermoelectric power experiments,[31] suggesting that oxygen transport within δ-Bi_2O_3 may be more complex than that of a simple vacancy mechanism. The substantially lower entropy compared to that of liquid Bi_2O_3 (Ref. 28) and the energetic preference for certain local entities (i.e., for example, the ⟨100⟩ and ⟨110⟩ oxygen-vacancy configurations are much lower in energy than the ⟨111⟩ alignment) indicate that the oxygen sublattice is not fully disordered and that (metastable) "microdomains" may exist within the δ phase.[23] In the extreme case of a fully ordered oxygen sublattice, the oxygens must migrate in a highly cooperative manner. It has also been suggested[32,33] that the high oxide-ion conductivity may result from a collective movement of domain walls of ordered "⟨110⟩ arrays" of oxygen vacancies.

The nature of the short-range order may also have an impact on the electronic properties of δ-Bi_2O_3 since, for example, the ⟨111⟩ oxygen-vacancy configuration is an electronic conductor whereas the ⟨110⟩ and ⟨100⟩ configurations possess semimetallic properties or a very small band gap of <0.1 eV.[20,26] In contrast, *ab initio* molecular dynamics (MD) simulations[34] suggest that δ-Bi_2O_3 possesses a distinct band gap. Furthermore, the possible presence of a stereochemically active lone pair, which is used to rationalize the highly distorted structures of many post-transition-metal compounds,[35] such as that of the ordered α phase of Bi_2O_3 itself, may also indicate the likelihood of substantial local distortions of the mobile and immobile sublattices associated with the large shifts into the 32(f) site[6] (see Fig. 2). This shift is much larger than the displacements that accompany the structural relaxations when optimizations are carried out by initially distributing the anions over the *ideal* 8(c) positions within the conventional 10-ion unit cell,[20,26] indicating that the 32(f) site may be associated with distinct minima on the potential-energy surface and thus serve as residential sites for the oxygens.

In a recent paper[34] we have presented a different model of the local structure of superionic Bi_2O_3 where the anion environment around the bismuths was found to be highly irregular, locally resembling the distorted "lone-pair" structures of many ordered post-transition-metal oxides (including the α and β phases of Bi_2O_3 itself). To put this view on firmer ground we carry out a detailed comparison with that of the β phase, which allows for a detailed insight into the structure of the mobile sublattice because the cationic sublattice of β-Bi_2O_3 is only slightly distorted from that of the fcc one. We carry out *ab initio* Born-Oppenheimer MD to probe the role of the local structure on the diffusion process within δ-Bi_2O_3 and how the dynamical local structure is connected to the electronic properties (i.e., the high polarizability of the immobile sublattice). Together with MD simulations, we also carry out extensive lattice static calculations by (1) quenching the dumped MD configurations at many different time steps and (2) using configurational (Boltzmann) averaging (CA).[36–38] CA is a direct Monte Carlo algorithm for the calculation of ensemble averages where local energy minima configurations are sampled at random and Boltzmann weighted. Previous studies have demonstrated the application of the CA method for modeling disordered oxides, minerals, and alloys.[36–40] Of particular advantage here is the insight gained into the superionic state by the comparison of calculations carried out in the static limit and MD simulations, which address the individual contributions arising from lattice vibrations and static disorder.

II. THEORY

Molecular dynamics simulations were carried out on the Born–Oppenheimer surface, where the electronic degrees of freedom are minimized at each ionic step.[41] The atomic movements are described using Nosé dynamics within the *NVT* ensemble and a Nosé thermostat was used. Computational details are given in the next section.

The CA method has been presented in detail in previous work (see, for example, Refs. 36, 37, and 39), and we shall here only briefly present the basic ingredients. Since interba-

TABLE I. Optimized structural parameters for β-Bi_2O_3. The data were extracted using the crystallographic package PLATON (Ref. 48).

Space group			$P\bar{4}2_1c$		
Lattice parameters			a=8.06 Å		
			c=5.70 Å		
Unit-cell volume			V=372 Å^3		
Bi-O distances (Å)	2.16	2.17	2.35	2.36	2.66
O-Bi-O angles (deg)	67.9	71.7	81.3	87.8	88.5
	90.9	97.2	116.3	140.2	173.9

sin events (oxygen diffusion) and intrabasin movements (vibrations) occur at different times[42,43] (see also discussion in Section IV E), we can map the configurational space by distributing the oxygens at random over a suitable grid followed by structural optimizations (i.e., rapid quenches) of each individual configuration. The cell volume, the cell shape, and the basic atomic coordinates were fully relaxed in all optimizations. In contrast to previous theoretical studies of short-range order within δ-Bi_2O_3,[20–24,26] where preferential arrangements for the oxygen vacancies were modeled by distributing the oxygens on the ideal 8(c) site *only*, we distribute oxygens over both the 8(c) and the 32(f) sites i.e., at (0.25, 0.25, 0.25), (0.375, 0.375, 0.375), etc., respectively (see Fig. 1), but with the constraint that a given tetrahedral cavity [which contains one 8(c) and four 32(f) positions] is occupied by maximum one oxygen. This choice provides a fairly uniform and unbiased grid for the extraction of ensemble averages and is motivated by the experimental evidence of a markedly distorted oxygen sublattice.[6,18,19] Ensemble averages (i.e., the average structure) over K randomly chosen optimized configurations are given as

$$\langle Y^{\text{static}} \rangle = \frac{\sum_{l=1}^{K} Y^l \exp\left(\frac{-E^l}{k_B T}\right)}{\sum_{l=1}^{K} \exp\left(\frac{-E^l}{k_B T}\right)}, \tag{2.1}$$

where E^l is the minimized potential energy of arrangement l and k_B is Boltzmann's constant. Configurational averaging resembles that of a random sampling Monte Carlo although the *important points*, i.e., the local minima, are sampled, rather than some random points within the basins on the potential-energy surface, providing a direct and highly efficient route for extracting the Boltzmann distribution in the static limit. We have previously shown that surprisingly few optimized arrangements are required for the accurate calculation of ensemble averages at high temperature when a significant fraction of all minima is thermally accessible.[39,44]

III. COMPUTATIONAL DETAILS

Ten individual *ab initio* Born-Oppenheimer molecular dynamics simulations and 50 structural optimizations were carried out within a $2\times2\times2$ (80-ion) unit cell where the conventional 10-ion unit cell was doubled along each crystallographic axis. For direct comparison, the MD simulations of the β phase were carried out in an 80-ion cubic unit cell constructed by transforming the crystallographic axis from the tetragonal (20-ion) unit cell using

$$\begin{pmatrix} a_\beta \\ b_\beta \\ c_\beta \end{pmatrix} = \begin{pmatrix} 1 & 1 & 0 \\ -1 & 1 & 0 \\ 0 & 0 & 1 \end{pmatrix} \begin{pmatrix} a_\delta \\ b_\delta \\ c_\delta \end{pmatrix}. \tag{3.1}$$

The α and β phases were optimized using the conventional 20-ion unit cells. Structural parameters of the β phase are presented in Table I and are in overall good agreement with results from our ND experiment.[13]

Initial extensive test calculations were carried out within the conventional (10-ion) cell by optimizing all symmetrically distinct oxygen configurations[45] constructed by the initial distribution of the ions over both the 8(c) and 32(f) sites (see previous section). This set of configurations includes the three oxygen-vacancy alignments, ⟨100⟩, ⟨110⟩, and ⟨111⟩, shown in Fig. 2 where only the 8(c) site is initially occupied. Many of these 10-ion optimizations converged to symmetrically equivalent configurations, and we found a total of 18 symmetrically distinct optimized oxygen arrangements (excluding the ⟨100⟩, ⟨110⟩, and ⟨111⟩ oxygen-vacancy configurations).

In all calculations we use the Perdew-Burke-Ernzerhof functional[46] for the calculation of the exchange-correlation contribution to the total energy as implemented in VASP (Refs. 41 and 47) with the $6s^26p^3$ and $2s^22p^4$ electron configurations for the bismuths and oxygens, respectively. We found that the explicit inclusion of the outer core d shells of the bismuths (the 5d states) had very little effect on the structural properties (e.g., the pair distribution functions and the conductivity) consistent with previous investigations of the chemical bond of the three idealized vacancy arrangements of δ-Bi_2O_3.[20,24]

The energy cutoff, E_{cut}, was 400 eV in the MD simulations, whereas the structural optimizations and the calculations of the electronic densities of states (DOSs) were carried out using E_{cut}=500 eV. All structural optimizations were followed by an additional rerelaxation to minimize distortions in the plane-wave basis associated with volume changes during the structural optimizations.

The Brillouin zone was sampled at the gamma point in the 80-ion MD simulations, and a $2\times2\times2$ Monkhorst-Pack (MP) grid was used for the optimizations of the 80-ion con-

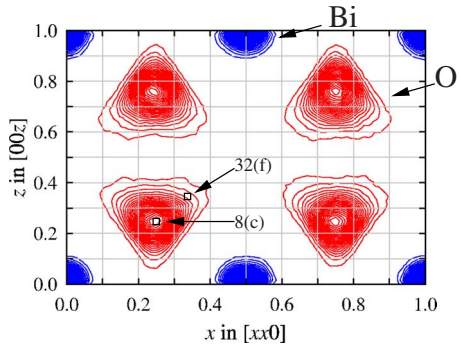

FIG. 3. (Color online) The ionic density of δ-Bi_2O_3 from MD at 1033 K, shown as a slice through the $(1\bar{1}0)$ plane. The refined 8(c) and 32(f) sites (taken from Ref. 13) are marked in the figure.

figurations. For the optimizations carried out within the 10-ion cell (including the three oxygen-vacancy alignments) and for the α phase we used a $4\times4\times4$ MP grid. For the β phase, a $4\times4\times6$ MP grid was used. In the MD simulations of β-Bi_2O_3, the unit-cell volume was consistent with that of ND experiment,[13] as discussed above, but the cell parameters were slightly adjusted such that the 80-ion simulation cell was cubic with the cell length, $a,=11.05$ Å. The cell volume used in the MD simulation of the δ phase was fixed at the value given by the CA simulations at 1033 K, i.e., the unit-cell length was $a_\delta=11.3$ Å, which is in excellent agreement with that of ND at 1033(3) K.[13] This choice was also partly motivated by the difficulty in choosing an equilibrium volume for a soft and highly disordered material such as δ-Bi_2O_3. Thus to examine the sensitivity of the properties to changes in the cell volume, additional test calculations were carried out by increasing the cell volume by up to 10%. Each MD simulation ran for 40 ps including equilibration periods of between 2 and 10 ps with a step length of 2 fs. With this choice of step length, the drift in the total energy is less than 0.3 meV ps^{-1} $atom^{-1}$.

A detailed analysis of the electronic density of states has been performed by decomposing the individual bands into contributions with distinct angular-momentum l numbers, by projecting the wave functions onto spherical harmonics within the Wigner-Seitz spheres defined by $r_{WZ}(Bi)<1.65$ Å and $r_{WZ}(O)<1.55$ Å. This choice is consistent with the cell-volume and the charge-density maps.

IV. RESULTS AND DISCUSSION

A. Ionic density profiles for δ-Bi_2O_3

The extreme disorder within the oxygen sublattice of δ-Bi_2O_3 and a highly flexible immobile sublattice are clearly seen in the average ionic density distributions shown in Fig. 3. The oxygens are "spread out" within the tetrahedral cavities possessing broad peaks at the 8(c) site and marked tetrahedral distortion in the ⟨111⟩ directions. The density profiles are in excellent agreement with that of ND-RMC,[13] although the Debye-Waller thermal clouds are less diffused. Interestingly, no distinct peaks are found in the ionic density near the 32(f) site consistent with the density profile in our recent ND-RMC study.[13] This differs from that of the average structural model[13] and previously reported density profiles for δ-Bi_2O_3,[18,19] where local maxima in the anionic density distribution are found near the 32(f) site.

Comparison with the optimized configurations carried out within 10-ion and 80-ion unit cells allows us to learn more about the topography of the underlying potential-energy surface and how the highly diffuse anionic density distribution is connected to the dynamics of the oxygens. The optimizations carried out using a 10-ion simulation cell are accompanied by substantial orthorhombic and tetragonal cell distortions. Typically, one of the axis is substantially elongated or shortened compared to the other two. The optimized cell volumes of the 10-ion configurations differ by as much as 20%. In contrast, the cell shape of the 80-ion configurations remains overall cubic upon optimization, and the cell volumes of the different optimized configurations differ by less than 6%. This suggests that most of the atom correlations is encapsulated within a 80-ion cell. In all these optimizations the oxygens relax appreciably from their ideal 8(c) site when initially distributed over *both* the 8(c) and the 32(f) sites. This confirms that the marked shift into the 32(f) site is attributable to extensive configurational disorder. The likelihood of considerable distorted local oxygen environments around the bismuths has also been suggested in a recent *ab initio* DFT study[49] by the inspection of a selection of "quasirandom" configurations. Here,[49] the oxygens were distributed over the 8(c) positions such as to match the correlation functions of an "infinite" (randomly chosen) configuration, followed by structural optimizations.

The presence of locally distorted sublattices implies that the dynamics of the oxygens within a tetrahedral cavity (metabasin) involves rapid "jumps" into and out of shallow basins on a highly undulating potential-energy surface. The diffuse anionic density distributions and the large relaxations accompanying the structural optimizations are consistent with the highly diffused density profile obtained experimentally (ND-RMC) (Ref. 13) and contrast those of previous theoretical investigations[20–26] where the structural optimization were typically accompanied by modest relaxations if all oxygens were initially distributed over the ideal 8(c) positions *only*.

B. Local structural models and thermodynamic properties of δ-Bi_2O_3

The distribution of the minimized energies of the 50 optimized arrangements constructed by the initial distribution of oxygens and vacancies over the 8(c) and 32(f) sites is shown in Fig. 4. We also plot the energies of the 10-ion optimizations where the three "idealized" alignments (shown in Fig. 2) are explicitly marked, along with those of the α and β phases and the superstructure reported in Ref. 21. Of particular note is that all 18 optimized 10-ion configurations, all 50 optimized 80-ion arrangements, and all quenched MD configurations [marked as "All (10-ions cell)," "random selection (80-ions cell)" and "quenched MD" in Fig. 2] lie *below* the minimized energies of the three distinct oxygen-vacancy configurations (shown in Fig. 2).

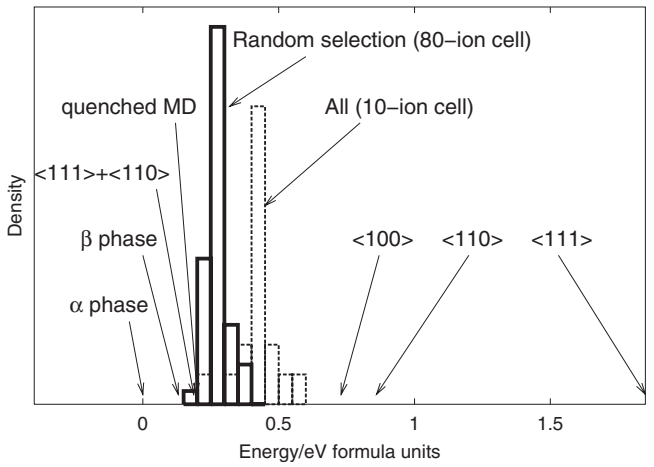

FIG. 4. Distributions of minimized energies found by optimizing configurations where the oxygens are initially distributed over both 8(*c*) and 32(*f*) sites (as described in Sec. II). Results using 10-ion and 80-ion cells are the histograms marked as "all (10-ion cell)" (dashed lines) and "random selection (80-ion cell)" (thick full lines), respectively. "All" denotes that all symmetrically distinct arrangements are optimized, excluding the "⟨100⟩," "⟨110⟩," and "⟨111⟩" arrangements (see Fig. 2), which are marked separately as "⟨100⟩," "⟨110⟩," and "⟨111⟩." The average energy calculated in the static limit by quenching a number of MD configurations is marked as "quenched MD." The "⟨111⟩+⟨110⟩" represents the superstructure reported in Ref. 21. All minimized energies are compared to that of α-Bi_2O_3, which is set to 0.0 eV.

The minimized energy of the β phase lies 0.13 eV (per formula unit) above that of the α phase in good agreement with the transition enthalpy, $\Delta H(\beta \rightarrow \alpha)$, obtained experimentally [$\Delta H(\beta \rightarrow \alpha) = -0.09$ eV (per formula unit)].[50] The average enthalpy for δ-Bi_2O_3 calculated using Eq. (2.1) at 1033 K and by minimizing the energy of 10 dumped configurations along the MD trajectories are in excellent agreement and ~0.2 eV/f.u. higher than that of the α phase. These values are in good agreement with the transition enthalpy $\Delta H(\alpha \rightarrow \delta)$ obtained experimentally [0.31 eV/f.u. at 1003 K (Ref. 28)] and a recent *ab initio* DFT study[49] (~0.4 eV/f.u.). The ⟨100⟩, ⟨110⟩, and ⟨111⟩ configurations are all much higher in energy than the transition enthalpy calculated above in the static limit (by, i.e., 0.5, 0.7, and 1.6 eV/f.u., respectively) and are unlikely to be thermally accessible within the bulk. However, the possibility for modeling the structure of δ-Bi_2O_3 using ordered low-energy superstructures has been suggested[21,23] by embedding a ⟨111⟩ configuration within a ⟨110⟩ array (marked as "⟨111⟩+⟨110⟩" in the figure). Although low in energy, comparison with CA emphasizes that a single ordered low-energy 80-ion configuration of the type suggested in Ref. 21 does not capture the essential structural [i.e., the large shift into the 32(*f*) site[34]] and thermodynamical features [i.e., the high configurational entropy of δ-Bi_2O_3 (Ref. 28)] of the disordering process, which involves a thermal average of many markedly different local low-energy "motifs" where the O^{2-} and Bi^{3+} are relaxed significantly away from their ideal average lattice sites. This is visualized in Fig. 5 where we show an example of a thermally accessible (local minima) configuration with

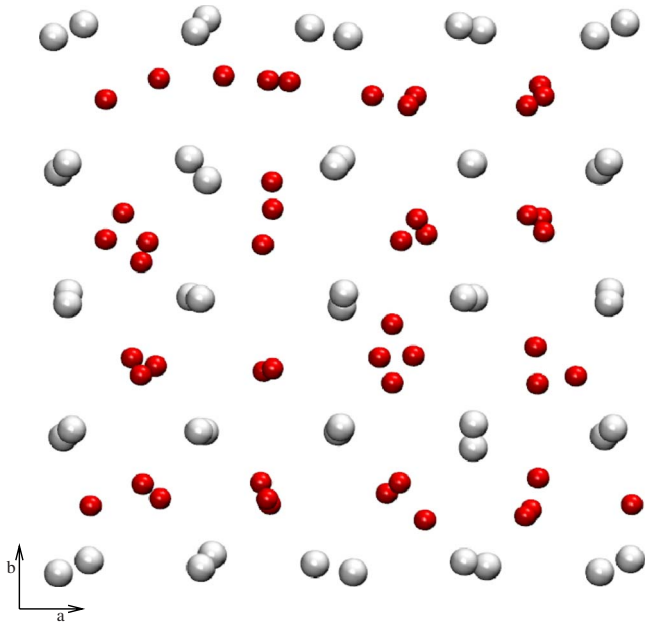

FIG. 5. (Color online) An example of an optimized low-energy configuration. The big white spheres are the bismuths, whereas the small red spheres are the oxygens.

energy ~0.05 eV (per formula unit) lower than the "⟨111⟩ +⟨110⟩" superstructure.[21]

C. Pair distribution and angular distribution functions

To obtain further insight into the local structure and atom correlations within β-Bi_2O_3 and δ-Bi_2O_3, we plot in Fig. 6 the radial (pair) distributions functions, $g_{BiBi}(r)$, $g_{OO}(r)$, and $g_{BiO}(r)$ and in Fig. 7 the distribution of angles, $A_{BiBiBi}(\theta)$, $A_{OOO}(\theta)$, and $A_{OBiO}(\theta)$. Results from MD and CA simulations for δ-Bi_2O_3 are reported at $T = 1033$ K together with MD results of β-Bi_2O_3 at 297 K.

The first peak in $g_{BiO}(r)$ of the δ phase, located at 2.2 (MD) and 2.25 Å (CA), is markedly shorter (by ~0.4 Å) than that expected from the average ionic density profile (see Fig. 3 and Ref. 13), resembling closely that of the β phase. Although $g_{BiO}(r)$ of δ-Bi_2O_3 is slightly broadened in comparison with that of β-Bi_2O_3, their peak positions and overall shapes are very similar. The good agreement with $g_{BiO}(r)$ calculated from RMC of the total scattering data[13,34] is particularly encouraging confirming the presence of strikingly short Bi-O bonds. Further discrepancies from that expected from the average ionic density distributions are also seen in $A_{OBiO}(\theta)$, which has a broad peak at $\cos(\theta) = 0.3$. This corresponds to O-Bi-O angles in the range of 70–80° and is consistent with a highly asymmetric anionic environment around the Bi^{3+} *locally* resembling those of the ordered α and β phases of Bi_2O_3 (for a detailed discussion of the angular distribution functions of δ-Bi_2O_3 from ND, see Ref. 13).

Investigating further the local environments of the bismuths by integrating the first peak in the Bi-O pair distribution function up to its first minimum shows that the average number of oxygens around a Bi^{3+} is, as expected, ~6 [5.9 (MD) and 5.7 (CA)]. However a time-resolved analysis (car-

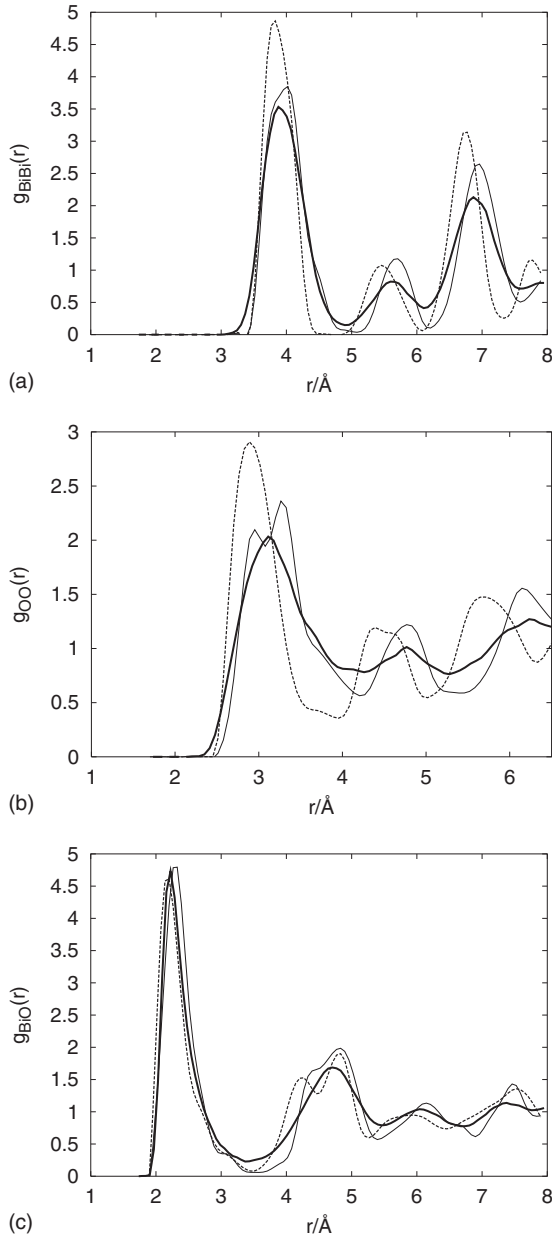

FIG. 6. Top, middle and bottom figures show the $g_{BiBi}(r)$, $g_{OO}(r)$, and $g_{BiO}(r)$, respectively. The thick and thin solid lines denote the MD and CA results for δ-Bi_2O_3 at 1033 K, respectively, whereas the dashed lines are the results for β-Bi_2O_3 at 297 K.

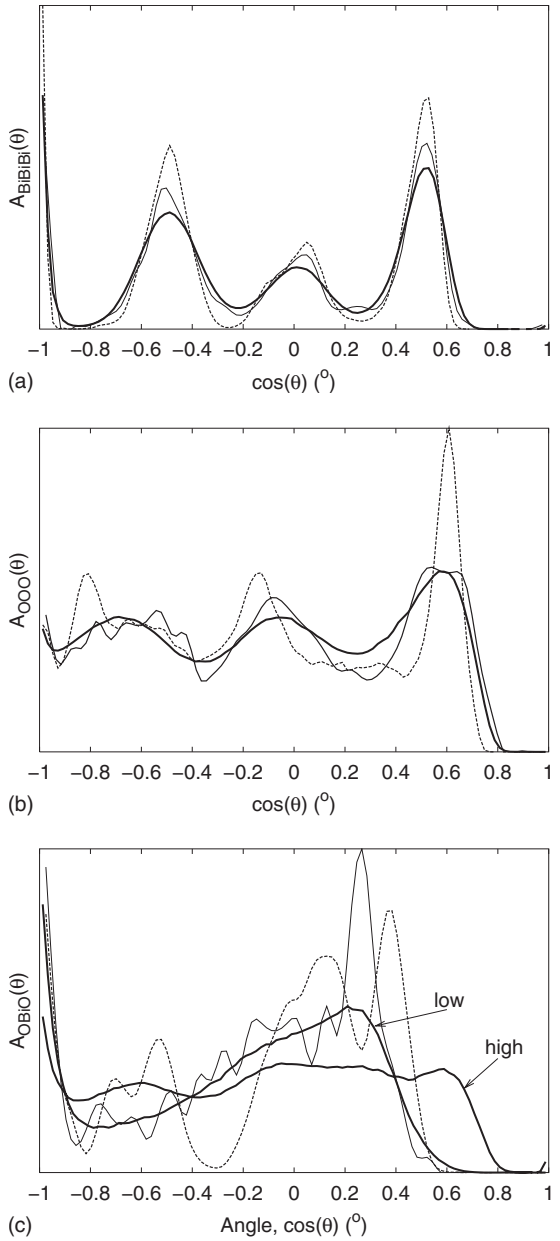

FIG. 7. Top, middle, and bottom figures show the $A_{BiBiBi}(\theta)$, $A_{OOO}(\theta)$, and $A_{OBiO}(\theta)$, respectively. The thick and thin solid lines denote the MD and CA results for δ-Bi_2O_3 at 1033 K, respectively, whereas the dashed lines are the MD results for β-Bi_2O_3 at 297 K. Two different cutoffs were used for the calculation of the $A_{OBiO}(\theta)$ (MD) at 1033 K. These are marked as "low" [$A_{OBiO}(\theta)$ is calculated up to 3.5 Å] and "high" [$A_{OBiO}(\theta)$ is calculated up to 4.2 Å].

ried out by dumping the atomic coordinates along the trajectory) suggests that the bismuths take a range of coordination numbers. That is, we find that the $Bi^{3+}s$ are surrounded by four, five, six, and seven oxygens within their first coordination shells. This emphasizes the striking ability of the bismuths in accommodating the migrating oxygens under very different local environments, which facilitates rapid anion diffusion. The overall short-range order of the local structure is also seen in $A_{OBiO}(\theta)$; whereas the oxygens found within the first coordination shell of a given cation is constrained angularly (marked as "low" in Fig. 7) the outer oxygens located within the first and second coordination shells are rather loosely bound angularly, as is seen in Fig. 7 (marked as "high").

The peaks in $g_{OO}(r)$ of δ-Bi_2O_3 are broad compared to that of the β phase and consistent with the diffuse anionic density profile (Fig. 3) confirming the experimental evidence for a highly disordered mobile sublattice.[13] The broad, but pronounced, peak in $g_{OO}(r)$ at 3.0 Å as well as a peak near 109° in the $A_{BiOBi}(\theta)$ (not shown) are broadly consistent with that expected from the mean atomic densities (see Fig. 3) and indicate the presence of some local order within the mobile sublattice. We find no evidence for alignments of oxygens within the next-nearest and third-nearest coordination shells of a given oxygen. However, a broad but notable peak at

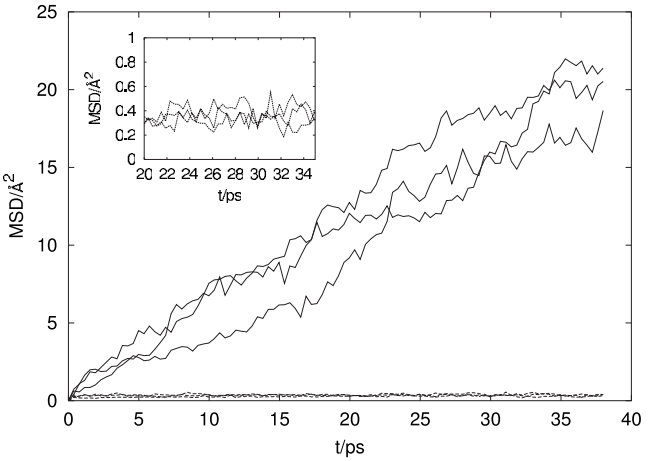

FIG. 8. The average MSD, $\frac{1}{N_{O/Bi}}\Sigma_{i=1}^{N_{O/Bi}}|\mathbf{r}_i(t)-\mathbf{r}_i(0)|^2$, for the oxygens (full lines) and the bismuths (dashed lines and inset). The results from three different MD simulations at 1033 K are shown.

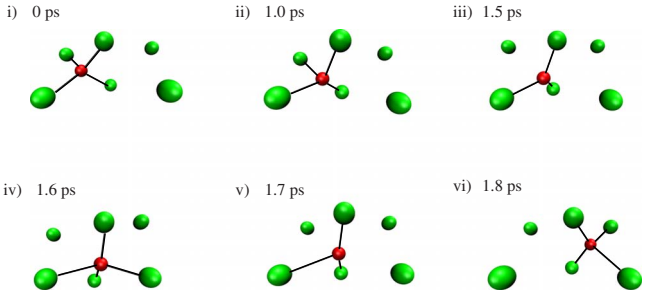

FIG. 9. (Color online) Various stages of a typical migrating oxygen (from MD) within δ-Bi_2O_3 at 1033 K. The snapshots are viewed along the ⟨010⟩ direction, and the nearest-neighboring bismuths involved in the diffusion are shown. The oxygen resides within a tetrahedral cavity (picture i) and starts to migrate (picture ii). Pictures (iii), (iv), and v) show that the oxygen resides at an "interstitial site" for a short time, where it carries out a few amplitudes of vibrations. Finally, the oxygen has fully migrated to the nearest-neighboring vacant cavity (picture vi).

around 6.0 Å is consistent with that obtained from ND-RMC,[13] indicating a tendency toward limited intermediate-range order within the oxygen sublattice.

The $A_{BiBiBi}(\theta)$ from MD possesses broad peaks at 70 and 120° consistent with a high-temperature fcc crystal lattice. Of particular note is the surprisingly broad $A_{BiBiBi}(\theta)$ peaks found in the static limit (CA) pointing to a structurally highly flexible and locally distorted immobile sublattice.

D. Diffusion coefficient of δ-Bi_2O_3

In Fig. 8 we plot the mean square displacements (MSDs), $\frac{1}{N_{O/Bi}}\Sigma_{i=1}^{N_{O/Bi}}|\mathbf{r}_i(t)-\mathbf{r}_i(0)|^2$, where $\mathbf{r}_i(t)$ and $\mathbf{r}_i(0)$ are the positions of the ith oxygen/bismuth at times t and 0 (after equilibration), and $N_{O/Bi}$ is the number of oxygens/bismuths in the simulation box. The MSDs show that we have captured the characteristic feature of solid electrolytes within the simulations; while the bismuths show no tendency of diffusion, the MSD of the oxygens increases roughly linearly with time. From the slope of the MSD of the oxygens we calculate the self-diffusion coefficients, D^O via the Einstein relation

$$D^O = \lim_{t\to\infty}\frac{1}{6tN_O}\left\langle\sum_{i=1}^{N_O}|\mathbf{r}_i(t)-\mathbf{r}_i(0)|^2\right\rangle, \qquad (4.1)$$

where the $\langle\cdots\rangle$ denotes a time average over the trajectory. We have not found any values of D^O from experiments within the literature, but the calculated value, $D^O=1.0\times10^{-5}$ cm^2 s^{-1}, is consistent with those of other superionic conductors with similar conductivities.[9]

E. Atomistic analysis of the trajectory of δ-Bi_2O_3

A detailed atomistic investigation of the characteristic times and possible diffusion mechanisms within δ-Bi_2O_3 has been carried out by dividing the simulation cell into distinct space-filling cubes (subcells),[42,51,52] with the cube center located at the tetrahedral 8(c) site, and the octahedral site located at alternate cube-corner positions. This choice is convenient for the interpretations of the ionic trajectories since most of the cationic density associated with a given tetrahedral cavity is encapsulated within a given subunit. Jumps can be therefore be identified when a oxygen "escapes" a given subcell. However, to distinguish jumps and vibrations with amplitudes stretching into a neighboring cavity, an oxygen is assumed to undergo diffusion if it has "left" its original cavity and carried out at least one vibration within the new subcell.

This analysis shows that the dynamics of the oxygens involves several distinct time scales. We find that the oxygens resides within the tetrahedral cavity for $\tau_{res}\sim 8$ ps. The distribution of vibrational frequencies extracted by Fourier transform of the velocity autocorrelation function shows that the oxygens vibrate with a period of ~0.1 ps, which is about 2 orders of magnitude lower than the average residence time. The flights between the tetrahedral cavities are rapid (~0.5 ps) or involve transient (short-lived) ~1 ps positions, where the migrating oxygens carry out a few vibrations near the octahedral 4(b) site. The trajectories show that the majority (~95%) of the oxygens migrate rapidly and decisively in the ⟨100⟩ direction. The marked bulges in the ⟨111⟩ directions in the cationic density profile (see Fig. 3) therefore show that the trajectories involving nearest neighboring cavities must be markedly *curved*. Indeed, a typical example showing different stages of a migrating oxygen is visualized in Fig. 9. It is interesting to note that, although the oxygens, while migrating, often reside near the octahedral site (see Fig. 9) they retain their low coordination environment at all stages during the diffusion. This emphasizes the striking ability of the bismuth sublattice to locally adapt such that an O^{2-} can easily escape its Madelung well and undergo diffusion to a neighboring vacant cavity.

The analysis of the trajectories carried out so far have only involved the consideration of single-particle events; that is, we have ignored the influence of the immobile lattice on the jumps of the oxygen and possible cooperative events among the oxygens. Thus, correlated movement has been investigated by comparing the calculated distribution of residence times with that expected from a random jump model (see Fig. 10). Whereas random uncorrelated events follows,

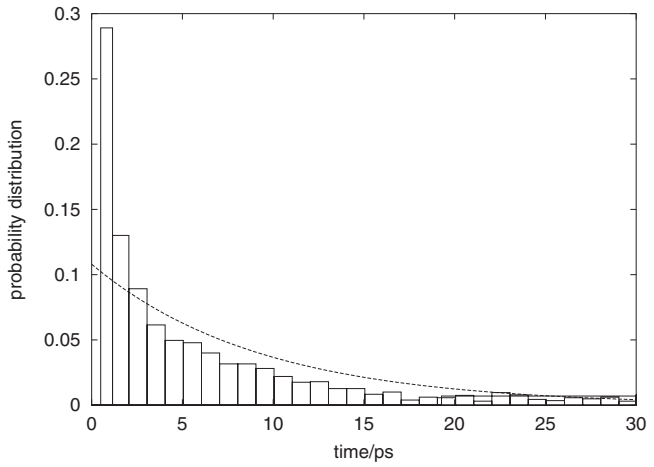

FIG. 10. Distribution of residence times of the oxygens (shown as bars) of δ-Bi_2O_3 at 1033 K (MD). The distribution of residence times expected from a random uncorrelated diffusion process calculated from Eq. (4.2) is shown as a dashed line. An oxygen is assumed to migrate to a neighboring basin (cell) if it remains within that basin (cell) for more than 0.5 ps (Ref. 52).

$$\bar{f}(\tau) = \frac{1}{\langle \tau_{\text{res}} \rangle} \exp(-\langle \tau_{\text{res}} \rangle), \tag{4.2}$$

correlated diffusion appears as a marked deviation from this behavior. As can be seen from Fig. 10, we find an unusually high occurrence of short residence times (<1.0 ps). To investigate the origin of this feature, we estimate the number of short residence oxygens that return to their previous cavity and compare this number to that expected if the short residence time oxygens were jumping to a random neighboring cavity (i.e., the relative number of "unsuccessful" jumps). Indeed, we found that 60% of all short residence oxygens returned to their original cavities, which accounts for about 95% of all cooperative events. This can be confirmed by calculating the diffusion coefficient from a simple jump diffusion model using $D'^{\text{O}}=1/6\nu_j b_O^2$, where $\nu_j=1/\tau_{\text{res}}$ is the jump frequency and b_O is the average jump distance between the nearest-neighboring lattice site. Inserting $\nu_j=1/8$ ps^{-1} above, we find $D'^{\text{O}}=2\times10^{-5}$ cm^2 s^{-1}, which is higher than that found via the Einstein relation using Eq. (4.1), confirming the likelihood of a significant number of unsuccessful jumps. Thus, there is little evidence of cooperative diffusion of oxygens, and we can estimate the oxide conductivity, σ, from

$$\sigma = 1/k_B e^2 \rho Q^{\text{O}} D^{\text{O}}, \tag{4.3}$$

where ρ and Q^{O} are the concentration and the formal charge of the ions, respectively. $D^{\text{O}}=1\times10^{-5}$ cm^2 s^{-1} is the anion self-diffusion coefficient found above from the MSD of the oxygens. The calculated σ, 0.2 Ω^{-1} cm^{-1}, is markedly lower that that measured experimentally, ~1 Ω^{-1} cm^{-1}(see Ref. 6). To investigate this in further detail we have carried out a number of additional MD simulations. Since, for example, we find a tendency of intermediate-range order within the mobile lattice and the likelihood of a large number of unsuccessful oxygen jumps, we carry out short MD simulations

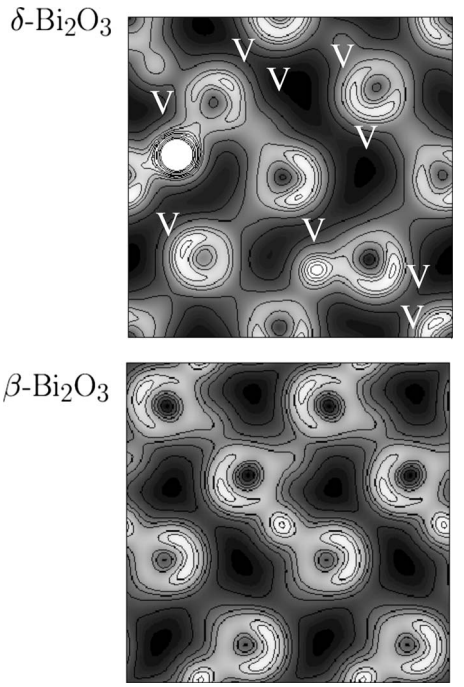

FIG. 11. Electron-density contour map of δ-Bi_2O_3 (top figure) and β-Bi_2O_3 (bottom figure) viewed along the $\langle 010 \rangle$ of the flourite crystal lattice. The contour map of δ-Bi_2O_3 is a snapshot from MD at 1033 K, whereas the contour map of β-Bi_2O_3 is the optimized structure. The plots display states from -12 to 0 eV, and contour levels are marked from 0.0 (black) to 0.5 $e/\text{Å}^3$ (white). The vacancies are marked as white "V"s for δ-Bi_2O_3. The Fermi energy is 0.0 eV.

($\sim$10 ps) using a larger supercell consisting of $3\times3\times3$ unit cells (containing 270 atoms) to check if the cell size may influence the dynamics of the oxygens. However the cell size appears to have no measurable effect on the ionic conductivity. Likewise, results from test calculations where we increase the cell volume by 10% indicate that the conductivity is not very sensitive to changes in the cell volume. Bearing in mind that the conductivity could be sensitive to small changes in the height of the barrier of migration we carry out additional MD simulations at somewhat higher temperature of 1200 K. Although, this corresponds to temperatures of liquid Bi_2O_3, we found no diffusion of the bismuths but a high superionic-like conductivity of the oxygens. This is consistent with the markedly lower ionic conductivity found in this work compared to that of experiment[6–8] and is not unusual for MD calculations carried out at the level of gradient-corrected DFT, although further test calculations are required to draw firm conclusions. It is also worth mentioning that we cannot rule out the possibility of the presence of "domains" and the possibility of enhanced ionic conductivity at interfaces between such domains.[33]

F. Electronic structure of β- and δ-Bi_2O_3

We now examine the nature of the Bi-O bond and the role of the highly polarizable immobile sublattice on the asymmetric local structure. In Fig. 11 we show representative con-

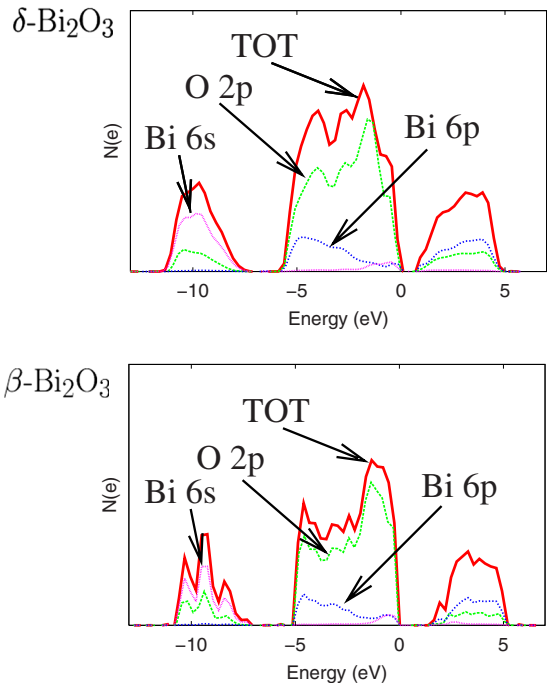

FIG. 12. (Color online) Total and partial electron density of states for δ-Bi_2O_3 (top figure) and β-Bi_2O_3 (bottom figure). The densities of states are calculated by averaging over the MD trajectory at 1033 and 297 K for the δ and β phases, respectively. The thick full red, dashed green, dotted purple, and dashed blue lines represent the total, the O 2*p*, the Bi 6*s*, and the Bi 6*p* states, respectively. The Fermi energy is 0.0 eV.

tour plots of the electronic density of δ-Bi_2O_3 and β-Bi_2O_3. A pronounced asymmetry is clearly visible near the Bi^{3+} nuclei (Fig. 11) with peaks in the direction of the vacancies (marked as white "V"s in the figure of δ-Bi_2O_3). This supports the presence of a stereochemically active "lone pair," and provides a plausible explanation for the highly irregular anion environments of the bismuths within the δ phase. The similarities between electron densities of the β and δ phases of Bi_2O_3 are striking. A stereochemically active lone pair has been suggested to play a central role in promoting the high ionic conductivity within δ-Bi_2O_3 (see, e.g., Ref. 53) and to explain the structural distortions of many fully ordered post-transition-metal oxides, including the α phase of Bi_2O_3 itself. However, the underlying hybridization that gives rise to this asymmetry is very different from that of the conventional (textbook) model where the presence of an inert "6*s* lone pair" is explained in terms of a directional 6*s*-6*p* hybrid orbital located near the Fermi level (see, e.g., Ref. 35). However, projecting the time-averaged density of states into distinct sites, orbital angular, and magnetic-moment quantum numbers, *l* and *m*, (see Fig. 12) shows that the states near the Fermi level, E_F, (from −2 to 0 eV) essentially constitutes the oxygen 2*p* orbitals with only small contributions from the bismuth 6*p*/6*s* states, whereas the majority of the 6*s* states is found at *bottom* of the valence band in good agreement with a recent *ab initio* DFT study.[49]

Interestingly, resolving the electron contour maps of δ-Bi_2O_3 in three distinct energy regions (see Fig. 13) defined by $-12 < E_{\text{bands}} < -7$ eV [Fig. 13(a)], $-7 < E_{\text{bands}} < -2$ eV [Fig. 13(b)], and $-2 < E_{\text{bands}} < 0$ eV [Fig. 13(c)] shows that the asymmetry of the electronic density around the Bi^{3+}, as seen in Fig. 11, does not arise from the 6*s* bands located at ~−10 eV but from the block of bands located near E_F. Whereas the electron density in the low-energy block (i.e., at −10 eV) is located at the atoms or concentrated in between the oxygens and the bismuths (not visible in the slice in Fig. 13), the lack of electron density in between the oxygens and the bismuths within $-2 < E_{\text{bands}} < 0$ eV indicates a pronounced antibonding interaction in this region. The dominant contribution of the 2*p* states near E_F may therefore play an important role in explaining the highly asymmetric electron density near the bismuth nuclei. To investigate this further, we analyze the characters of the bands located near the Fermi level. Indeed, *all* bands in this region constitute a mixture of O 2*p*, Bi 6*s*, and Bi 6*p* states; that is, we do not, for example, find bands that have a pure O 2*p* character or bands possessing particular large weights of Bi 6*s* and/or Bi 6*p* characters. Whereas the contribution from the Bi 6*p* is roughly constant at ~5% in the region $-2 < E_{\text{bands}} < 0$ eV the contribution to the bands from the Bi 6*s* states increases from about ~5% at −2 eV to about 12% at E_F.

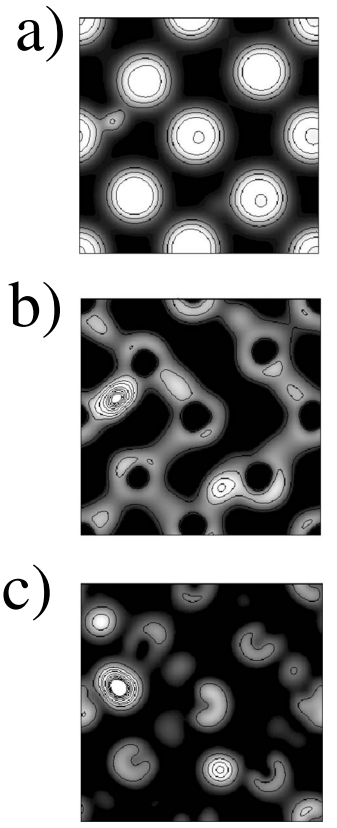

FIG. 13. Decomposed electron-density contour maps for δ-Bi_2O_3 taken from a typical MD time snapshot at 1033 K (viewed along the ⟨010⟩ direction). The three plots show the electronic density from bands with energy (a) from −12 to −7 eV, (b) from −7 to −2 eV, and (c) from −2 to 0 eV. Contour levels are displayed between 0.0 (black) and 0.15 $e/Å^3$ (white). The Fermi energy is 0.0 eV.

The pronounced influence of the oxygen 2*p* orbitals on the asymmetric electron density clearly contrasts with that of

the conventional lone-pair (textbook) model but is very similar to results from recent bonding analysis of structural distortions in selected ordered post-transition-metal compounds such as those of α-PbO and the α phase of Bi_2O_3 itself.[20,54] Indeed, in these ordered phases the majority of the 6*s* states are also located at the bottom of the valance band whereas the pronounced asymmetry in the electron density around the cations arises due to a hybridization of all O 2*p*, Bi 6*s*, and Bi 6*p* bands. The link between the distorted structures of ordered post-transition-metal oxides and the disordered high-temperature δ phase of Bi_2O_3 can be further confirmed by the comparison with that of β-Bi_2O_3. The characters of the bands near E_F of the optimized structure and of a selection of MD configurations, all contain a mixture of Bi 6*s* and Bi 6*p* and O 2*p* orbitals. The striking similarities between the electronic structure of the ordered post-transition-metal phases [i.e., α-PbO,[54] α-Bi_2O_3,[20] and β-Bi_2O_3 (Fig. 11)] and that of the highly disordered δ-Bi_2O_3 (Fig. 11) provide strong evidence for a revision of the conventional lone-pair model for modeling highly defective post-transition-metal oxides.

As shown in Fig. 12, striking similarities between the electronic structure of the disordered high-temperature phase and the ordered low-temperature phases of Bi_2O_3 (Ref. 20) are also reflected in the partial DOS, although the band gap of δ-Bi_2O_3 is smaller and the bands wider than that of the ordered α and β (see Fig. 12) phases of Bi_2O_3. In the case of β-Bi_2O_3, we find a distinct band gap of 1.7 eV, which is in fair agreement with an experimental estimate of 2.8 eV,[55] bearing in mind that DFT tends to systematically underestimate band gaps of semiconductors.[56] The presence of a distinct band gap of $\sim$0.7 eV (MD) and of $\sim$2.0 eV (CA) at the Fermi level (see Fig. 12) is consistent with experimental measurements of δ-Bi_2O_3 thin films[57] and stand in contrast to those of the three idealized anion-vacancy alignments,[20,24,26] which appear to possess metallic, semimetallic or a very small band gap of $\sim$0.1 eV. The substantially higher band gap found in the static limit is associated with the broadening of the bands when vibrations are taken into account. The band gap found in the static limit is in good agreement with the band gap found for the "superstructure" reported in Ref. 21 and those of selected "random structures" of oxygens[49] [which both predict band gaps of $\sim$2.0 eV (Refs. 21 and 49)].

The increase in the band gap accompanying the $\delta \rightarrow \beta$ transition is good agreement with that suggested in Ref. 24, where the δ phase was thought to have a substantially lower band gap of $\sim$1 eV compared to β-Bi_2O_3. This is entirely consistent with the presence of an ordered sublattice within β-Bi_2O_3 and a highly disordered sublattice within δ-Bi_2O_3.

V. CONCLUSION

In this work we have examined in detail the structural and dynamical properties of the β and δ phases of bismuth sesquioxide (Bi_2O_3) using Born-Oppenheimer *ab initio* molecular dynamics at the level of gradient-corrected DFT. Comparison of the two phases allows one to separate and identify the distinct structural and thermodynamic features of oxygen disorder within δ-Bi_2O_3 since the structural distortions of the immobile lattice accompanying the $\delta \rightarrow \beta$ transition are negligible.

The ionic density plots, the pair, and the bond angle distribution functions are in very good agreement with ND results reported in.[13] The short Bi-O bonds of $\sim$2.1–2.2 Å and the broad peaks in $A_{\text{O-Bi-O}}$ at $\sim$70° indicate that the bismuths within the δ phase possess highly irregular anion arrangements, locally resembling the distorted structures of many ordered post-transition-metal compounds under ambient conditions. This is exemplified here by the comparison with β-Bi_2O_3. A structurally "flexible" immobile sublattice is clearly evident from the broad peaks in g_{BiBi} and A_{BiBiBi}, and the bismuths are shown to take a range of coordination numbers. Comparison with extensive lattice static simulations carried out using configurational (Boltzmann) averaging and by optimizing a number of MD configurations show that these local distortions are largely attributable to the presence of "static" distorted mobile and immobile sublattices within δ-Bi_2O_3. This places some doubt on the validity of previous structural models based on a cubic environment in which O^{2-} vacancies are preferentially aligned in pairs in the $\langle 100 \rangle$, $\langle 110 \rangle$, and/or $\langle 111 \rangle$ directions, or distributed at random over these ideal tetrahedral positions. Whereas the average $\delta \rightarrow \beta$ transition enthalpy calculated in the static limit via CA and by averaging over a number of quenched MD configurations are in very good agreement with that obtained experimentally, the minimized energies of the idealized oxygen-vacancy configurations, where the oxygens are aligned in the $\langle 100 \rangle$, $\langle 110 \rangle$, or $\langle 111 \rangle$ directions are substantially higher by $>$0.5 eV/f.u. and unlikely to be thermally accessible within bulk δ-Bi_2O_3. We find that many of the 50 optimized 80-ion configurations [where the oxygens are initially distributed over both the 8(*c*) and 32(*f*) sites] are thermally inaccessible emphasizing a strong energetic preference for particular local structures.

Comparison of MD and lattice static calculations shows that the dynamics of the oxygens involves a highly undulating potential-energy surface. The movements *within* a distinct tetrahedral cavity (metabasin) involve rapid "jumps" into and out of shallow basins with times consistent with a typical optical phonon mode (with period of $\sim$0.1 ps) pointing to an unusual entropic contribution to the stability of the superionic phase. The stabilization is strongly linked to the striking ability of the bismuth to locally adapt such that an oxygen can easily escape its Madelung well and undergo diffusion to a neighboring vacant cavity.

Examination of the MD trajectories indicates that 95% of the "jumps" is in the $\langle 100 \rangle$ directions. The trajectories are markedly *curved* and the diffusion is strongly influenced by the presence of local distortions of the cation sublattice, as is evident from an unusually high occurrence of short residence time oxygens compared to that expected for uncorrelated diffusion. Many oxygens appear to migrate but, if the slowly vibrating cation sublattice does not possess the required degrees of freedom to accommodate the motion, the anion returns to its original cavity. In contrast, there is little evidence of correlations between the motions of different anions, i.e., the distributions of residence times $>$1 ps follows that expected for random, uncorrelated events.

The "soft" immobile lattice is intimately linked to the polarizability of the bismuths which is visualized in the elec-

tronic contour plots. This provides evidence for the presence of a stereochemically active, but chemically dynamic, "lone pair." Inspection of the bands show that this asymmetric charge distribution arises from the bands with energy near E_F, which possess a mixture of all oxygen 2*p*, bismuth 6*s*, and bismuth 6*p* orbitals. The influence of the oxygen 2*p* orbitals in mediating highly asymmetric electronic bismuth environments contrasts that of the conventional 6*s* lone-pair (textbook) model which has been used to explain the extreme ionic conductivity within the δ phase of Bi_2O_3 and for understanding the electronic origin of the structural distortion of many ordered post-transition-metal oxides. Our results show striking similarities to many of these compounds[20,54] providing further strong evidence for a revision of the conventional lone-pair model for studying also highly defective materials exemplified here by the extreme case of δ-Bi_2O_3.

*chrism@kjemi.uio.no

[1] P. Varotsos, Solid State Ionics **179**, 438 (2008).
[2] M. Faraday, Philos. Trans. R. Soc. London **1838**, 90.
[3] M. T. Hutchings, K. Clausen, M. H. Dickens, W. Hayes, J. K. Kjems, P. G. Schnabel, and C. Smith, J. Phys. C **17**, 3903 (1984).
[4] C. E. Derrington and M. O'Keeffe, Nature Phys. Sci. **246**, 44 (1973).
[5] J. P. Goff, W. Hayes, S. Hull, and M. T. Hutchings, J. Phys.: Condens. Matter **3**, 3677 (1991).
[6] H. A. Harwig, Z. Anorg. Allg. Chem. **444**, 151 (1978).
[7] T. Takahashi, H. Iwahara, and Y. Nagai, J. Appl. Electrochem. **2**, 97 (1972).
[8] T. Takahashi and H. Iwahara, J. Appl. Electrochem. **3**, 65 (1973).
[9] S. Hull, Rep. Prog. Phys. **67**, 1233 (2004).
[10] P. Shuk, H. D. Wiemhöfer, U. Guth, W. Göpel, and M. Greenblatt, Solid State Ionics **89**, 179 (1996).
[11] N. M. Sammes, G. A. Tompsett, H. Nafe, and F. Aldinger, J. Eur. Ceram. Soc. **19**, 1801 (1999).
[12] V. V. Kharton, F. M. B. Marques, and A. Atkinson, Solid State Ionics **174**, 135 (2004).
[13] S. Hull, S. T. Norberg, M. G. Tucker, S. G. Eriksson, C. E. Mohn, and S. Stølen (unpublished).
[14] L. G. Sillen, Ark. Kemi, Mineral. Geol. **12A**, 1 (1937).
[15] N. Cornei, N. Tancret, F. Abraham, and O. Mentre, Inorg. Chem. **45**, 4886 (2006).
[16] G. Gattow and H. Schröder, Z. Anorg. Allg. Chem. **318**, 176 (1962).
[17] B. T. M. Willis, Acta Crystallogr. **18**, 75 (1965).
[18] P. D. Battle, C. R. A. Catlow, J. Drennan, and A. D. Murray, J. Phys. C **16**, L561 (1983).
[19] M. Yashima and D. Ishimura, Chem. Phys. Lett. **378**, 395 (2003).
[20] A. Walsh, G. W. Watson, D. J. Payne, R. G. Edgell, J. Guo, P. A. Glans, T. Learmonth, and K. E. Smith, Phys. Rev. B **73**, 235104 (2006).
[21] D. S. Aidhy, J. C. Nino, S. B. Sinnott, E. D. Wachsman, and S. R. Phillpot, J. Am. Ceram. Soc. **91**, 2349 (2008).
[22] G. Zhong, J. Wang, Z. Dai, J. Wang, and Z. Zeng, Phys. Status Solidi B **246**, 97 (2009).
[23] P. W. M. Jacobs and D. A. MacDónaill, Solid State Ionics **23**, 270 (1987).
[24] N. I. Medvedeva, V. P. Zhukov, V. A. Gubanov, D. L. Novikov, and B. M. Klein, J. Phys. Chem. Solids **57**, 1243 (1996).
[25] P. W. M. Jacobs and D. A. MacDónaill, Solid State Ionics **23**, 279 (1987).
[26] J. M. Carlsson, B. Hellsing, H. S. Domingos, and P. D. Bristowe, Phys. Rev. B **65**, 205122 (2002).
[27] N. V. Skorodumova, A. K. Jonsson, M. Herranen, M. Strømme, G. A. Niklasson, B. Johansson, and S. I. Simak, Appl. Phys. Lett. **86**, 241910 (2005).
[28] H. A. Harwig and A. G. Gerards, Thermochim. Acta **28**, 121 (1979).
[29] S. Boyapati, E. D. Wachsman, and N. Jiang, Solid State Ionics **140**, 149 (2001).
[30] H. A. Harwig and A. G. Gerards, J. Solid State Chem. **26**, 265 (1978).
[31] J. H. W. D. Wit, T. Honders, and G. H. J. Broers, in *Fast Ion Trasnport in Solids*, edited by P. Vashishta, J. N. Mundy, and G. K. Shenoy (North Holland, Amsterdam, 1979).
[32] W. van Gool, J. Solid State Chem. **7**, 55 (1973).
[33] J. A. Kilner and J. D. Faktor, in *Progress in Solid Electrolytes*, edited by T. A. Wheat, A. Ahmad, and A. K. Kuriakose (Canada Centre for Mineral and Energy Technology, Ottawa, 1983).
[34] C. E. Mohn, S. Stølen, S. T. Norberg, and S. Hull, Phys. Rev. Lett. **102**, 155502 (2009).
[35] D. M. Adams, *Inorganic Solids* (John Wiley, London, 1974).
[36] N. L. Allan, G. D. Barrera, R. M. Fracchia, M. Y. Lavrentiev, M. B. Taylor, I. T. Todorov, and J. A. Purton, Phys. Rev. B **63**, 094203 (2001).
[37] I. T. Todorov, N. L. Allan, M. Y. Lavrentiev, C. L. Freeman, C. E. Mohn, and J. A. Purton, J. Phys.: Condens. Matter **16**, S2751 (2004).
[38] C. E. Mohn, N. L. Allan, C. L. Freeman, P. Ravindran, and S. Stølen, J. Solid State Chem. **178**, 346 (2005).
[39] C. E. Mohn and S. Stølen, J. Phys.: Condens. Matter **19**, 466208 (2007).
[40] C. Cienfuegos, E. P. Isoardi, and G. D. Barrera, Phys. Rev. B **71**, 144202 (2005).
[41] G. Kresse and J. Hafner, Phys. Rev. B **47**, 558 (1993).
[42] G. Jacucci and A. Rahman, J. Chem. Phys. **69**, 4117 (1978).
[43] J. Sarnthein, K. Schwarz, and P. E. Blöchl, Phys. Rev. B **53**, 9084 (1996).
[44] C. E. Mohn and S. Stølen, J. Chem. Phys. **123**, 114104 (2005).
[45] E. Bakken, N. L. Allan, T. H. K. Barron, C. E. Mohn, I. T. Todorov, and S. Stølen, Phys. Chem. Chem. Phys. **5**, 2237 (2003).
[46] J. P. Perdew, K. Burke, and M. Ernzerhof, Phys. Rev. Lett. **77**, 3865 (1996).
[47] G. Kresse and D. Joubert, Phys. Rev. B **59**, 1758 (1999).
[48] A. L. Spek, J. Appl. Crystallogr. **36**, 7 (2003).
[49] D. Music, S. Konstantinidis, and J. M. Schneider, J. Phys.: Condens. Matter **21**, 175403 (2009).

[50] C. N. R. Rao, G. V. S. Rao, and S. Ramdas, J. Phys. Chem. **73**, 672 (1969).
[51] S. Wengert, R. Nesper, W. Andreoni, and M. Parrinello, Phys. Rev. Lett. **77**, 5083 (1996).
[52] C. E. Mohn, S. Hull, and S. Stølen, J. Phys.: Condens. Matter (to be published).
[53] G. Marisse, in *Fast Ion Transport in Solids*, edited by B. Scrosati (Kluwer, Amsterdam, 1974).
[54] D. J. Payne, R. G. Egdell, A. Walsh, G. W. Watson, J. Guo, P. A. Glans, T. Learmonth, and K. E. Smith, Phys. Rev. Lett. **96**, 157403 (2006).
[55] V. Dolocan, Appl. Phys. (Berlin) **16**, 405 (1978).
[56] M. Shishkin, M. Marsman, and G. Kresse, Phys. Rev. Lett. **99**, 246403 (2007).
[57] K. Laurent, G. Y. Wang, S. Tusseau-Nenez, and Y. Leprince-Wang, Solid State Ionics **178**, 1735 (2008).